Electronic Supplementary Material (ESI) for Energy & Environmental Science.

Supporting Information

Electric-field-driven Interfacial Trapping of Drifting Triboelectric Charges via Contact Electrification

Jin-Kyeom Kim[a,‡], Gi Hyeon Han[b,‡], Sun-Woo Kim[a], Hee Jun Kim[a], Rahul Purbia[a], Dong-Min Lee[a], Jong Kyu Kim[c], Hee Jae Hwang[d], Hyun-Cheol Song[a,e], Dukhyun Choi[d], Sang Woo Kim[a,f], Zhong Lin Wang[g], and Jeong Min Baik[a,e,f*]

[a]School of Advanced Materials Science and Engineering, Sungkyunkwan University (SKKU), Suwon 16419, Republic of Korea.

[b]School of Materials Science and Engineering, Ulsan National Institute of Science and Technology (UNIST), Ulsan 44919, Republic of Korea.

[c]Department of Materials Science and Engineering, Pohang University of Science and Technology (POSTECH), 77 Cheongam-ro, Nam-gu, Pohang 37673, Republic of Korea.

[d]School of Mechanical Engineering, College of Engineering, Sungkyunkwan University, 2066, Seobu-ro, Jangan-gu, Suwon, Gyeonggi 16419, South Korea.

[e]KIST-SKKU Carbon-Neutral Research Center, Sungkyunkwan University (SKKU), Suwon 16419, Republic of Korea.

[f]SKKU Institute of Energy Science and Technology (SIEST), Sungkyunkwan University, Suwon 16419, Republic of Korea.

[g]School of Materials Science and Engineering, Georgia Institute of Technology, Atlanta, 30332-0245, Georgia, USA.

‡These authors contributed equally to this work

*Corresponding author at: School of Advanced Materials Science and Engineering, Sungkyunkwan University (SKKU), Suwon 16419, Republic of Korea.

E-mail address: jbaik97@skku.edu (J. M. Baik).

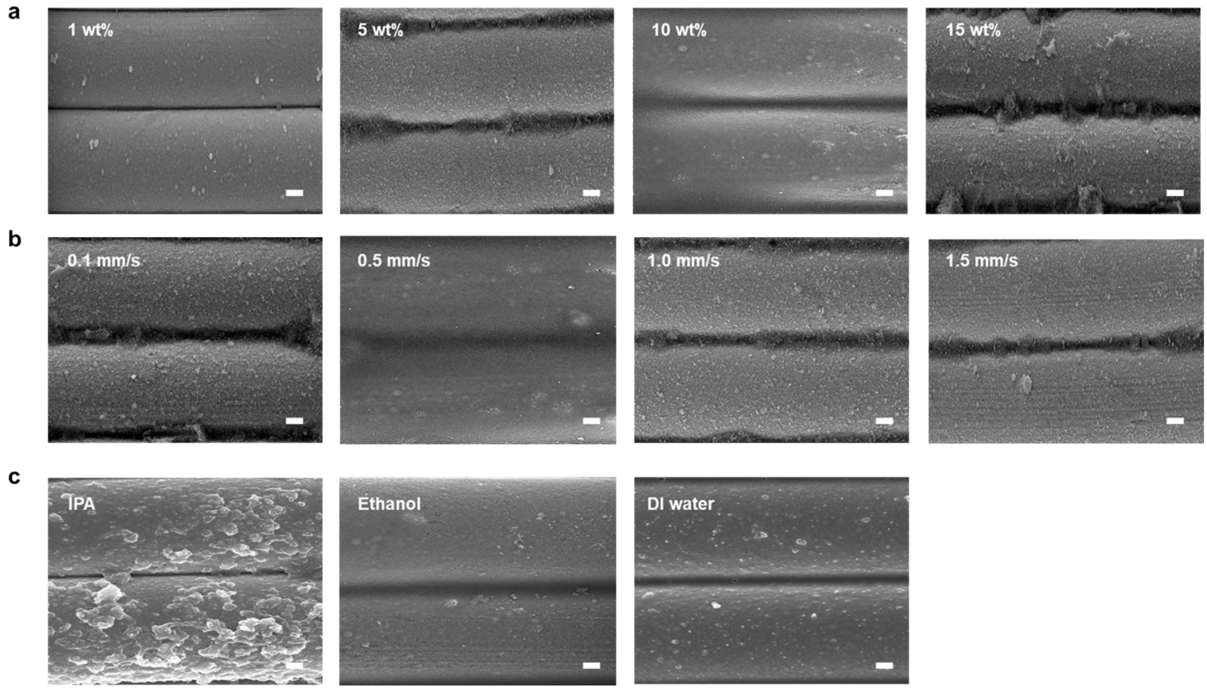

Figure S1. The SiO_2 NPs can be optimized by considering several parameters onto the Ni-mesh via the dip-coating process. (a) Concentration of SiO_2 NPs (1wt%, 5wt%, 10wt% and 15wt%), (b) Lifting speed (0.1 mm/s, 0.5 mm/s, 1.0 mm/s and 1.5 mm/s), (c) Capillary force during the solvent evaporation process (IPA, ethanol and di water). Scale bar: (a-c) 2 μm SEM images.

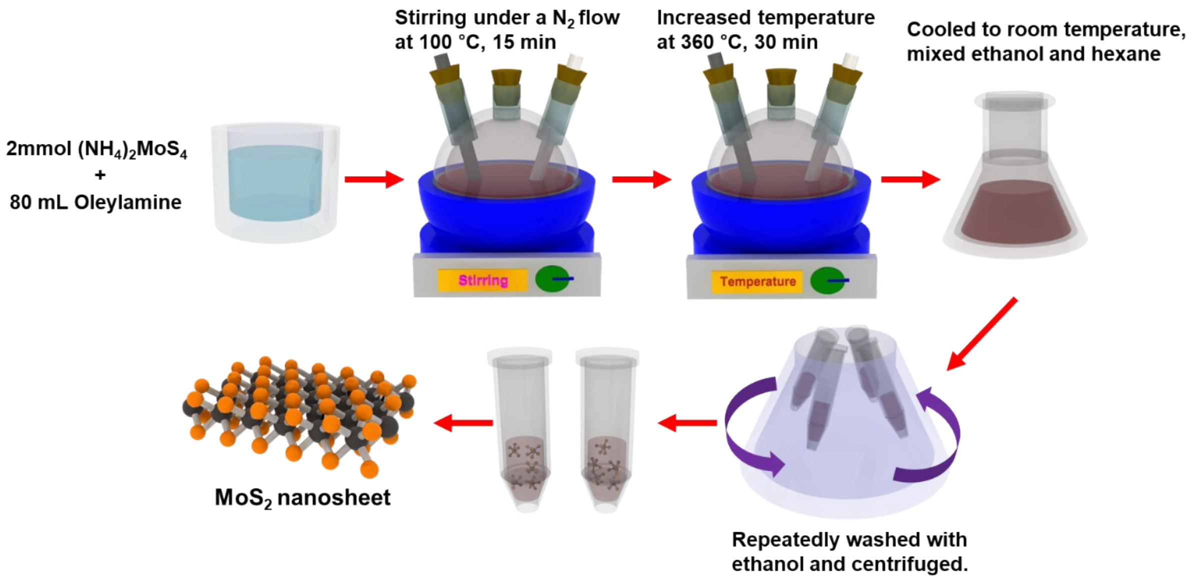

Figure S2. MoS_2 nanosheets (NSs) were synthesized through a heat-up method using an ammonium molybdate ($(NH_4)_2MoS_4$) as a precursor with oleylamine as a reducing solvent).

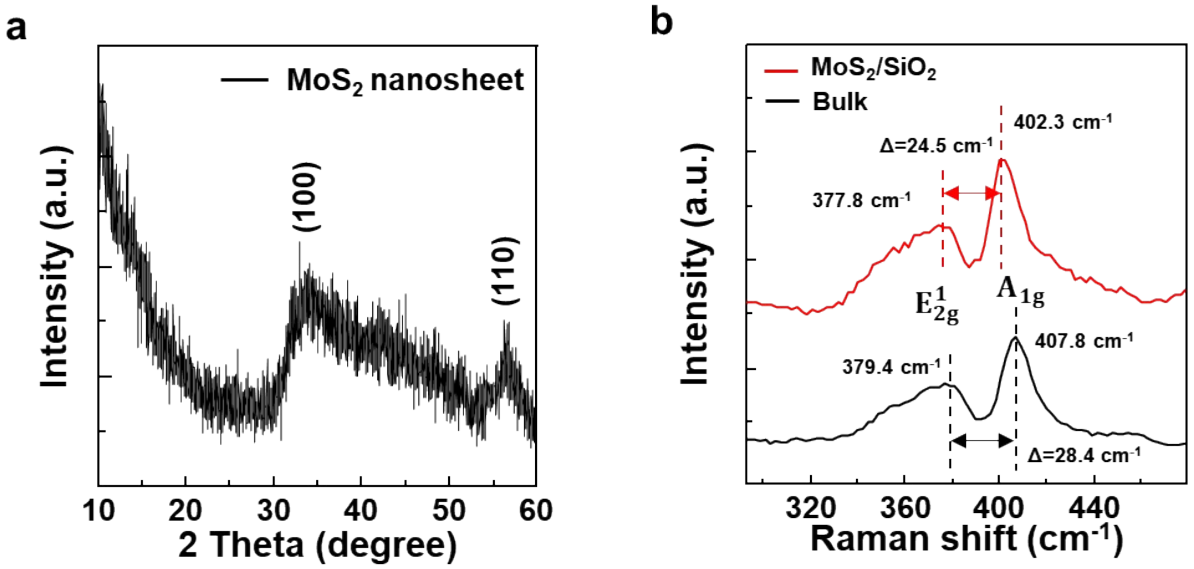

Figure S3. The characteristics of MoS_2 nanosheet. (a) X-ray diffraction (XRD) patterns of the MoS_2. (b) Raman spectra of the MoS_2/SiO_2 and bulk MoS_2.

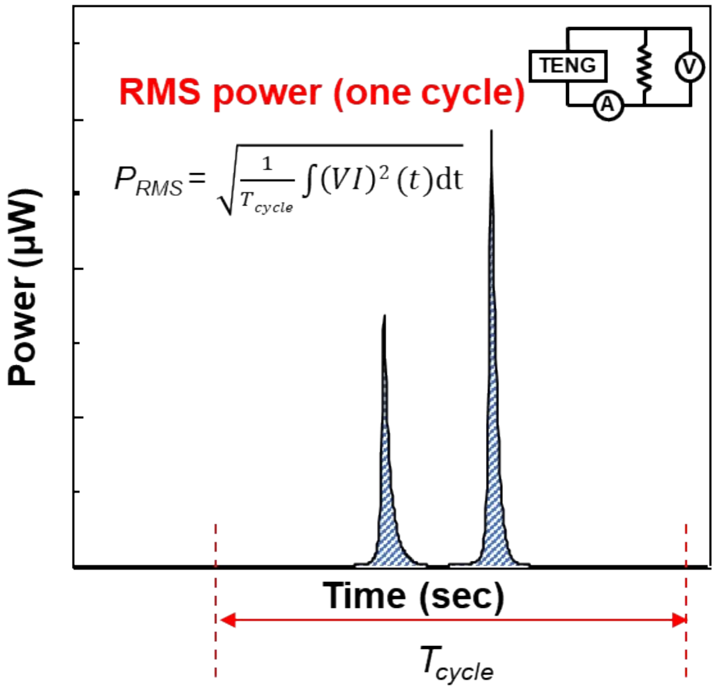

Figure S4. In this study, Root mean square (RMS) calculation method used for power measurement.

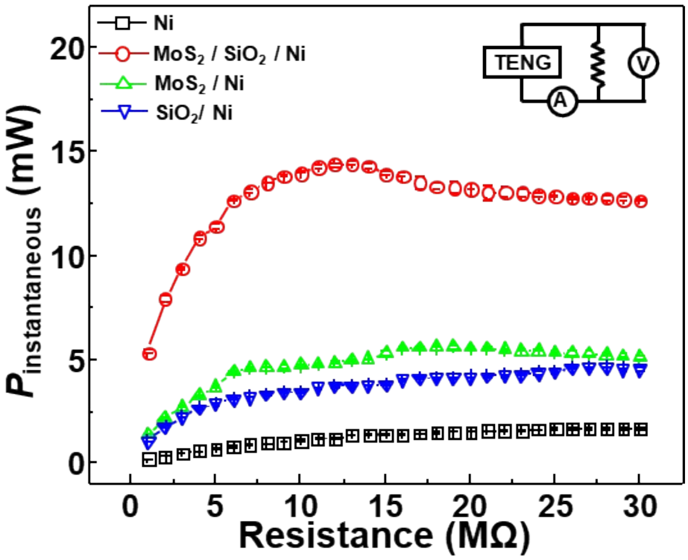

Figure S5. The instantaneous power of the TENG with external loads ranging from 1 to 30 MΩ with different cationic materials: Ni; SiO_2/Ni; MoS_2/Ni; MoS_2/SiO_2/Ni.

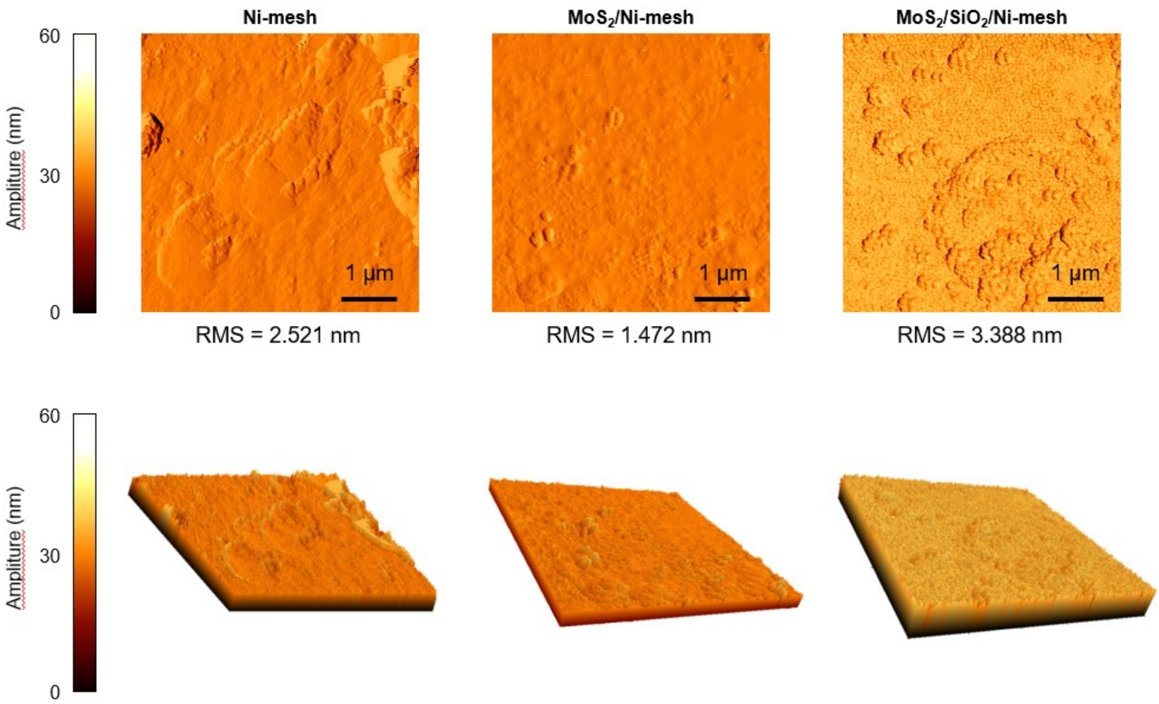

Figure S6. 2-dimensional and 3-dimensional AFM images of Ni, MoS_2/Ni, and MoS_2/SiO_2/Ni.

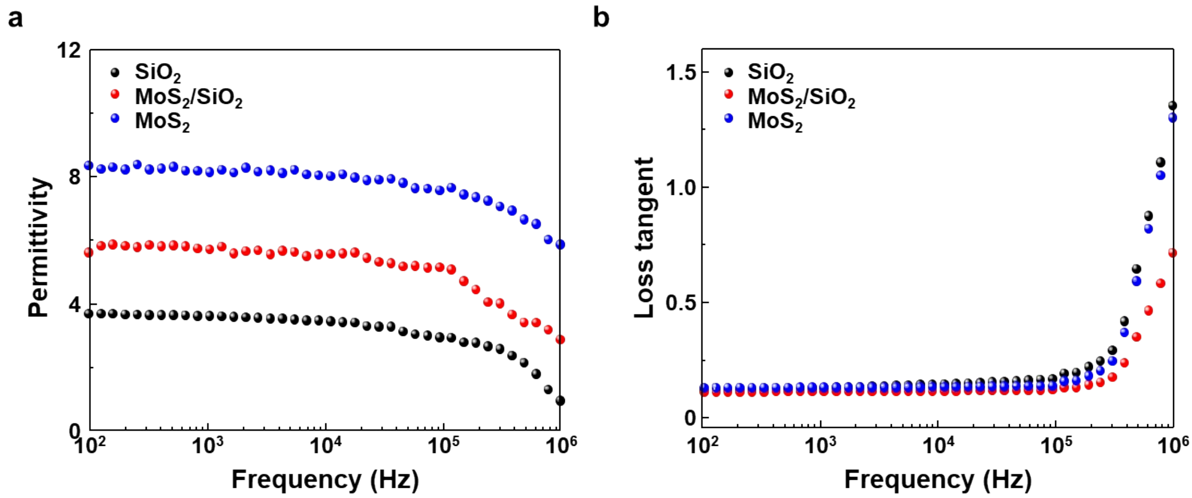

Figure S7. The frequency-dependent dielectric properties of cationic materials. (a) The frequency-dependent dielectric constant, and (b) dielectric loss properties of the cationic materials over the frequency range of 10^2 to 10^6 Hz at room temperature.

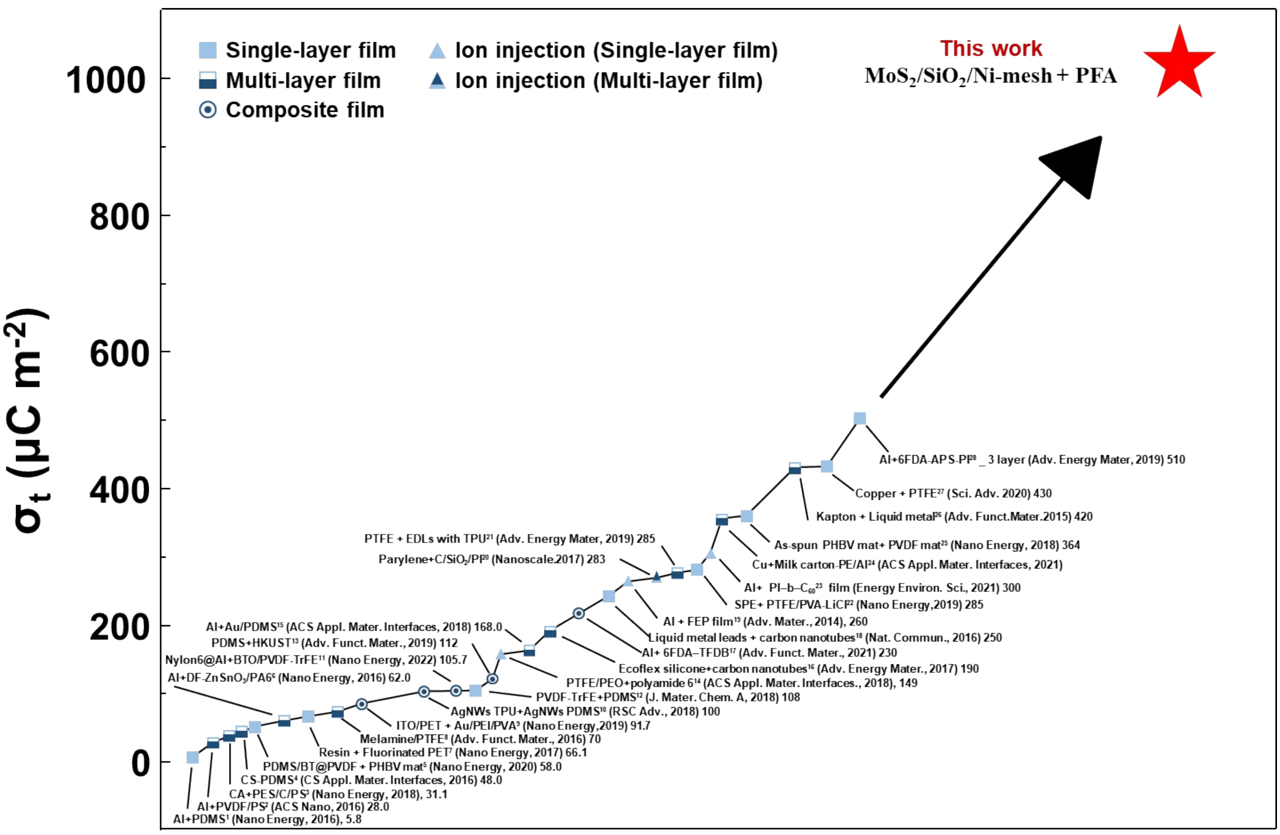

Figure S8. The state-of-the-art materials resulted charge densities reported recently in top journals, compared with this work in this manuscript.

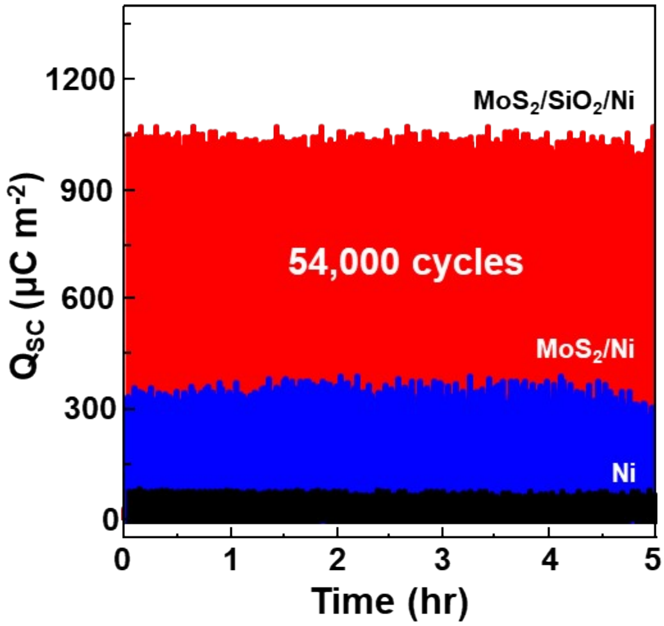

Figure S9. Durability test of the TENG under cycled compressive force of 30 N over 54,000 cycles. The Q_{sc} of the TENGs fabricated PFA and Ni, MoS_2 /Ni, and $MoS_2/SiO_2/Ni$ as a function of measuring time.

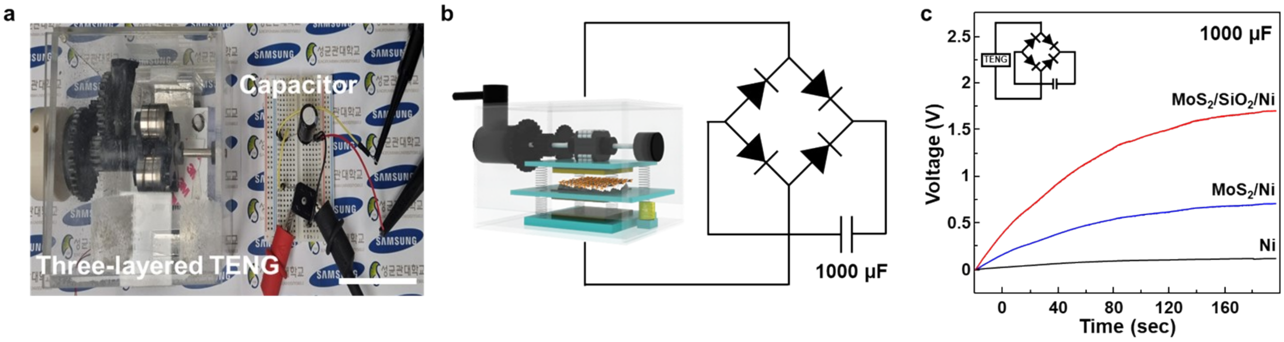

Figure S10. Charging process of the three-layered triboelectric nanogenerator. (a) The real photo with scale bar of 3 cm and (b) circuit composed of the three-layered TENG, a rectifier and a capacitor (1000 μF). (c) Charging process of the 1000 μF capacitor by the different cationic materials such as Ni, MoS_2/Ni, and MoS_2/SiO_2/Ni.

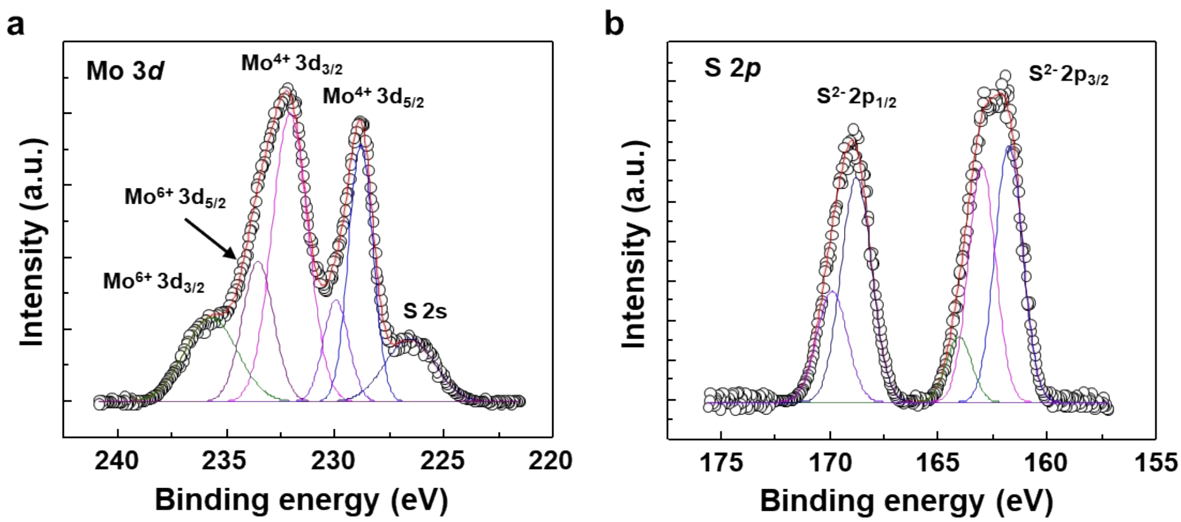

Figure S11. Comparison of the XPS spectra of (a) Mo 3*d* and (b) 2*p* core-level.

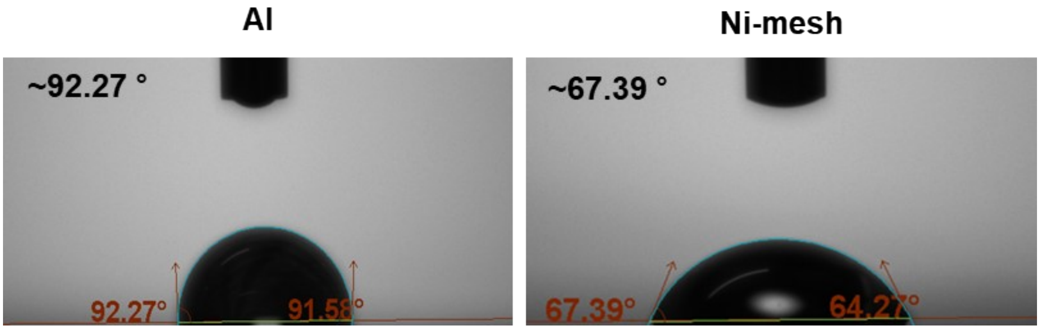

Figure S12. Side-view goniometer images during static contact angle measurement at the surface of Al, Ni and Ni-mesh.

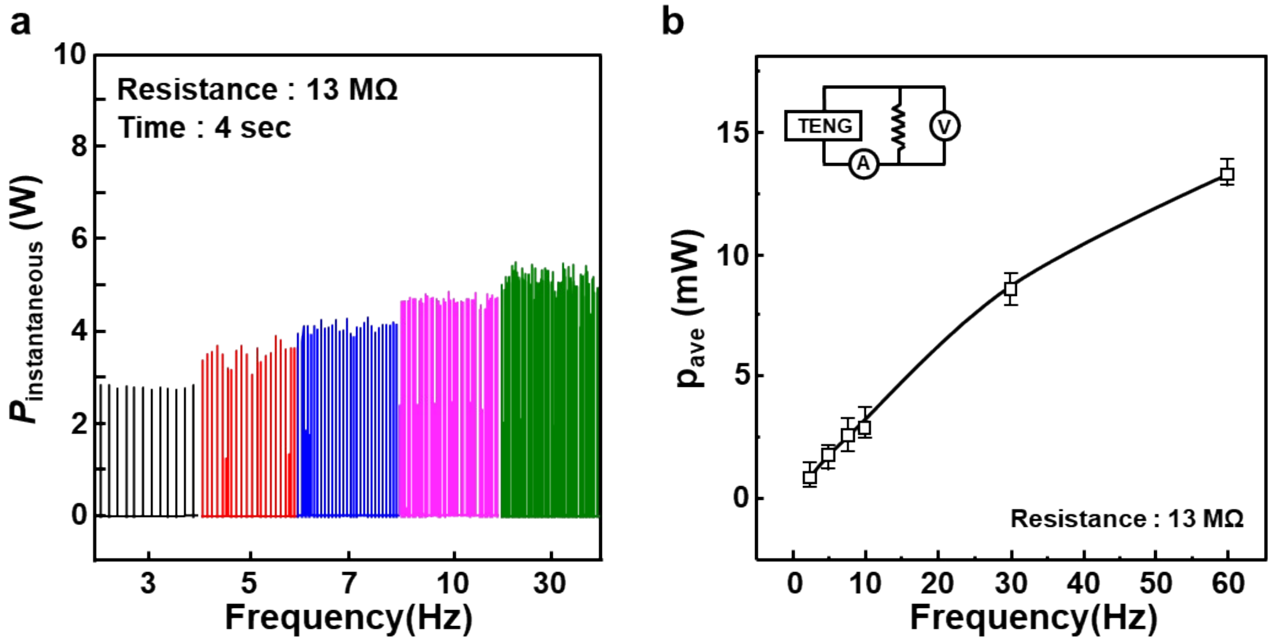

Figure S13. Power generated by the $MoS_2/SiO_2/Ni$ based TENG with three-layered structure. (a) The instantaneous power and (b) the P_{RMS} of the TENG with different frequency from 3 to 60 Hz at 13 MΩ.

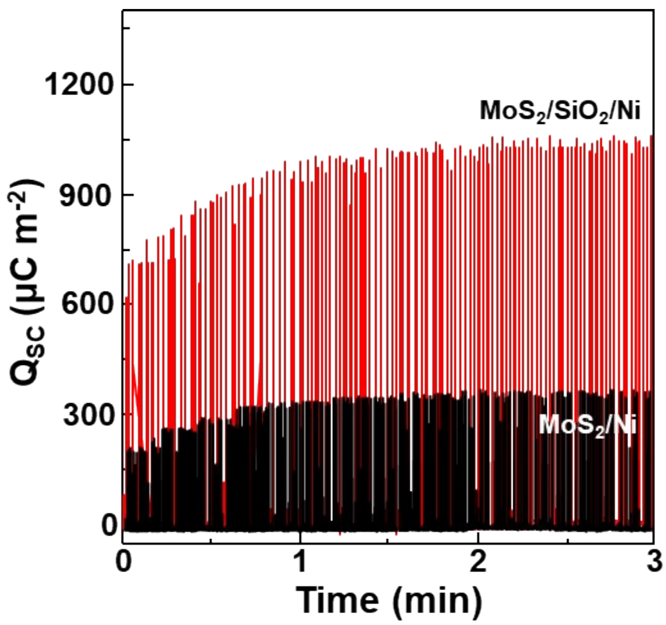

Figure S14. The Q_{sc} of the TENG with MoS_2/Ni and MoS_2/SiO_2/Ni for saturation under cycled compressive force of 30 N over 540 cycles.

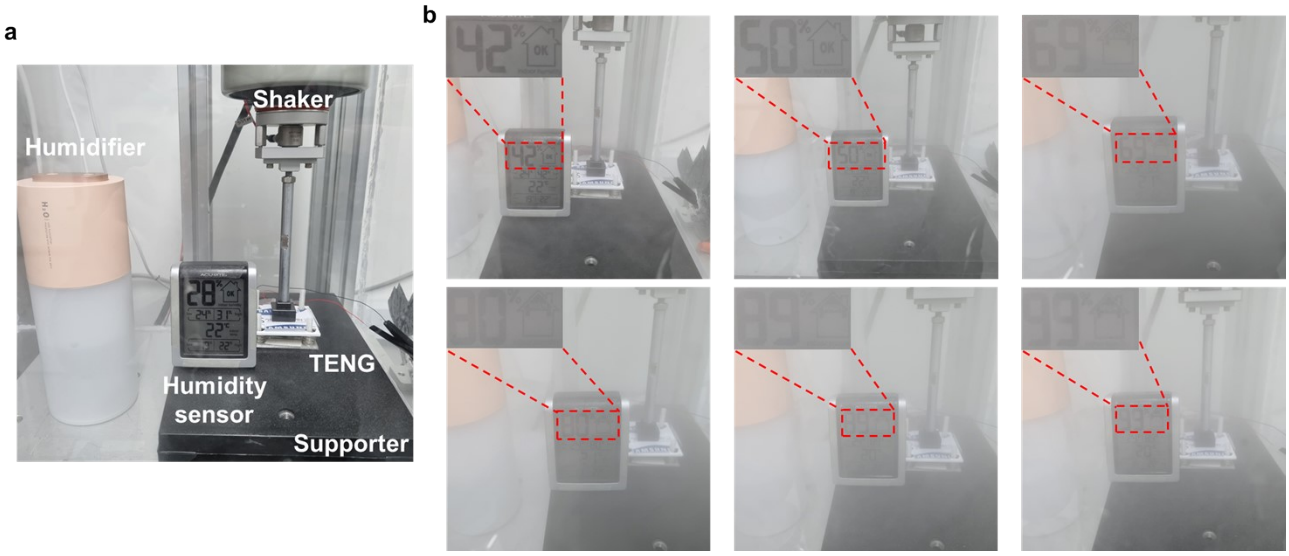

Figure S15. (a) Photographs of the humidity system composed of supporter, shaker, humidifier, and humidity sensor. (b) Photographs of the RH value from 42 % to 99 % using humidity sensor.

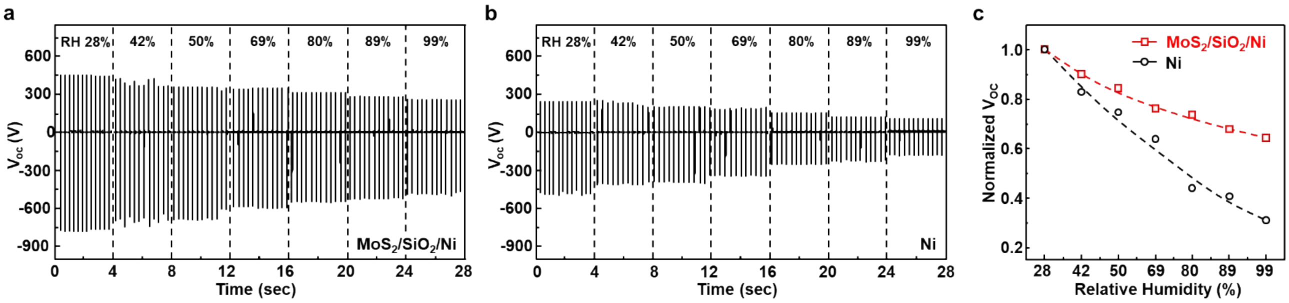

Figure S16. The V_{oc} generated by TENG as a function of relative humidity from 28 % to 99 % (a) $MoS_2/SiO_2/Ni$; (b) Ni. (c) The normalized V_{oc}.

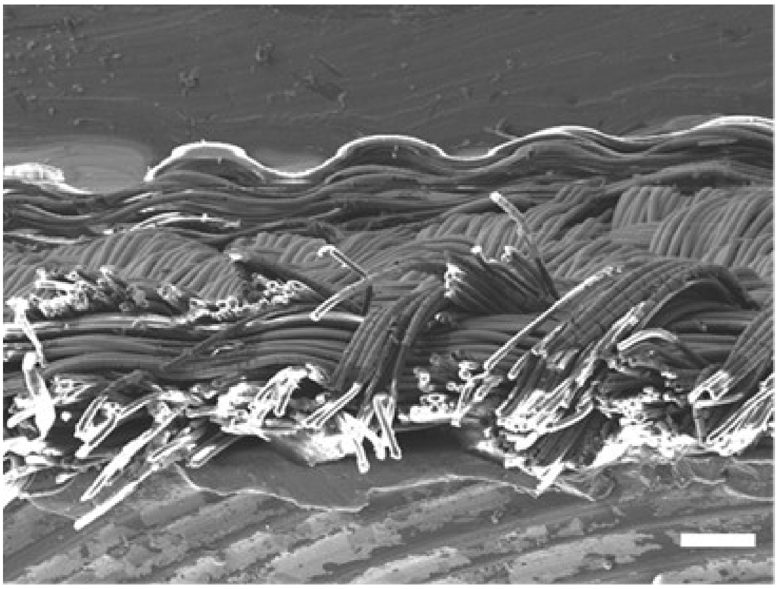

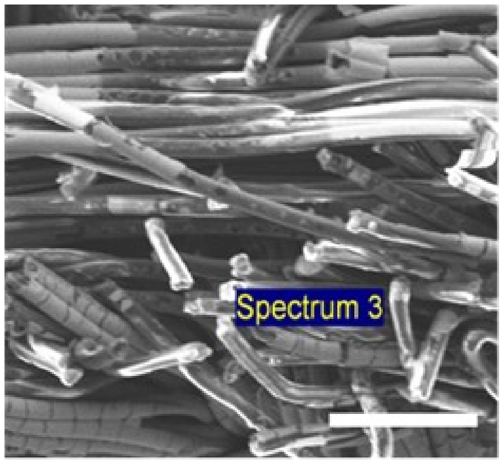

Element	Weight%	Atomic%
C K	72.26	77.63
O K	27.74	22.37

Figure S17. The field-emission scanning electron microscope (FE-SEM) images of Ni-mesh. The cross-sectional view of Ni-mesh and EDS result (scale bar: 100 μm).

Supplementary Notes

Supplementary Note 1. The energy conversion efficiency (ECE, η) of the triboelectric nanogenerator.

In general, the conversion efficiency is defined as the ratio between the output energy and the input energy, in which the output energy is produced by the TENG and the input energy is the energy applied to the TENG. Here, as an input energy, kinetic energy (E_k) can be defined with the velocity (v) and mass (m) of top layer and calculated as $\frac{1}{2}mv^2$. Assuming that the acceleration is constant, the velocity (v) of the top layer with the frequency was monitored by using a video camera (2.81 m/s) and the mass (m) was estimated as the mass (80 g) of the top layer, in which the mass of Al film and perfluoroalkoxy alkanes (PFA) layer are negligible.

i) Input energy (kinetic energy)

$E_{kinetic} = \frac{1}{2}mv^2 = 315.8\ \mu J$

ii) Output energy (electric energy)

$E_{electric} = Q = \int_{t_1}^{t_2} I^2 R\, dt = 51.9\ \mu J$

iii) Energy conversion efficiency (η)

$$\eta = \frac{E_{electric}}{E_{kinetic}} \times 100\ (\%) = \frac{51.9\ \mu J}{315.8\ \mu J} \times 100\ (\%) = 16.5\ \%$$

Thus, the kinetic energy is 315 μJ under a compressive force of 30 N. With an external load resistance of 13 MΩ, the calculated energy per a cycle reached approximately 51.9 μJ. The energy conversion efficiency was also calculated to be approximately 16.5 % according to the calculation method suggested before.[1-5] However, the mass of the top layer may be not correct because the top layer was contacted by the pushing tester.

References

1 C. Jin, D. S. Kia, M. Jones and S. Towfighian, *Nano Energy*, 2016, **27**, 68–77.

2 N. Cui, L. Gu, Y. Lei, J. Liu, Y. Qin, X. Ma, Y. Hao and Z. L. Wang, *ACS Nano*, 2016, **10**, 6131–6138.

3 B. Yu, H. Yu, T. Huang, H. Wang and M. Zhu, *Nano Energy*, 2018, **48**, 464–470.

4 J. Chen, H. Guo, X. He, G. Liu, Y. Xi, H. Shi and C. Hu, *ACS Appl. Mater. Interfaces*, 2016, **8**, 736–744.

5 X. Zhang, S. Lv, X. Lu, H. Yu, T. Huang, Q. Zhang and M. Zhu, *Nano Energy*, 2020, **75**, 104894.

6 N. Soin, P. Zhao, K. Prashanthi, J. Chen, P. Ding, E. Zhou, T. Shah, S. C. Ray, C. Tsonos, T. Thundat, E. Siores and J. Luo, *Nano Energy*, 2016, **30**, 470–480.

7 H. S. Wang, C. K. Jeong, M.-H. Seo, D. J. Joe, J. H. Han, J.-B. Yoon and K. J. Lee, *Nano Energy*, 2017, **35**, 415–423.

8 H. Zhu, N. Wang, Y. Xu, S. Chen, M. Willander, X. Cao and Z. L. Wang, *Adv. Funct. Mater.*, 2016, **26**, 3029–3035.

9 L. Wang, X. Yang and W. A. Daoud, *Nano Energy*, 2019, **55**, 433–440.

10 H. Niu, X. Du, S. Zhao, Z. Yuan, X. Zhang, R. Cao, Y. Yin, C. Zhang, T. Zhou and C. Li, *RSC Adv.*, 2018, **8**, 30661–30668.

11 B. Chai, K. Shi, H. Zou, P. Jiang, Z. Wu and X. Huang, *Nano Energy*, 2022, **91**, 106668.

12 Z. Fang, K. H. Chan, X. Lu, C. F. Tan and G. W. Ho, *J. Mater. Chem. A*, 2018, **6**, 52–57.

13 R. Wen, J. Guo, A. Yu, J. Zhai and Z. lin Wang, *Adv. Funct. Mater.*, 2019, **29**, 1807655.

14 P. Zhao, N. Soin, K. Prashanthi, J. Chen, S. Dong, E. Zhou, Z. Zhu, A. A. Narasimulu, C. D. Montemagno, L. Yu and J. Luo, *ACS Appl. Mater. Interfaces*, 2018, **10**, 5880–5891.

15 M. Lai, B. Du, H. Guo, Y. Xi, H. Yang, C. Hu, J. Wang and Z. L. Wang, *ACS Appl. Mater. Interfaces*, 2018, **10**, 2158–2165.

16 S. Li, J. Wang, W. Peng, L. Lin, Y. Zi, S. Wang, G. Zhang and Z. L. Wang, *Adv. Energy Mater.*, 2017, **7**, 1602832.

17 X. Tao, S. Li, Y. Shi, X. Wang, J. Tian, Z. Liu, P. Yang, X. Chen and Z. L. Wang, *Adv. Funct. Mater.*, 2021, **31**, 2106082.

18 J. Wang, S. Li, F. Yi, Y. Zi, J. Lin, X. Wang, Y. Xu and Z. L. Wang, *Nat. Commun.*, 2016, **7**, 12744.

19 S. Wang, Y. Xie, S. Niu, L. Lin, C. Liu, Y. S. Zhou and Z. L. Wang, *Adv. Mater.*, 2014, **26**, 6720–6728.

20 J. J. Shao, W. Tang, T. Jiang, X. Y. Chen, L. Xu, B. D. Chen, T. Zhou, C. R. Deng and Z. L. Wang, *Nanoscale*, 2017, **9**, 9668–9675.

21 H. J. Hwang, J. S. Kim, W. Kim, H. Park, D. Bhatia, E. Jee, Y. S. Chung, D. H. Kim and D. Choi, *Adv. Energy Mater.*, 2019, **9**, 1803786.

22 L. Shi, S. Dong, H. Xu, S. Huang, Q. Ye, S. Liu, T. Wu, J. Chen, S. Zhang, S. Li, X. Wang, H. Jin, J. M. Kim and J. Luo, *Nano Energy*, 2019, **64**, 103960.

23 J. W. Lee, S. Jung, J. Jo, G. H. Han, D.-M. Lee, J. Oh, H. J. Hwang, D. Choi, S.-W. Kim, J. H. Lee, C. Yang and J. M. Baik, *Energy Environ. Sci.*, 2021, **14**, 1004–1015.

24 Y. Li, Z. Zhao, Y. Gao, S. Li, L. Zhou, J. Wang and Z. L. Wang, *ACS Appl. Mater. Interfaces*,

2021, **13**, 30776–30784.

25 Z. Li, M. Zhu, Q. Qiu, J. Yu and B. Ding, *Nano Energy*, 2018, **53**, 726–733.

26 W. Tang, T. Jiang, F. R. Fan, A. F. Yu, C. Zhang, X. Cao and Z. L. Wang, *Adv. Funct. Mater.*, 2015, **25**, 3718–3725.

27 A. Chen, C. Zhang, G. Zhu and Z. L. Wang, *Adv. Sci.*, 2020, **7**, 2000186.

28 J. W. Lee, S. Jung, T. W. Lee, J. Jo, H. Y. Chae, K. Choi, J. J. Kim, J. H. Lee, C. Yang and J. M. Baik, *Adv. Energy Mater.*, 2019, **9**, 1901987.

29 G. Xu, D. Guan, J. Fu, X. Li, A. Li, W. Ding and Y. Zi, *ACS Appl. Mater. Interfaces*, 2022, **14**, 5355–5362.